

Monolayer Structure of Supramolecular Antagonistic Salt Aggregates

David Jung,[†] Jens Harting,^{*,†,‡} and Marcello Sega^{*,†}

[†]*Helmholtz Institute Erlangen-Nürnberg for Renewable Energy, Forschungszentrum Jülich, Fürther Straße 248, 90429 Nürnberg, Germany.*

[‡]*Department of Chemical and Biological Engineering and Department of Physics, Friedrich-Alexander-Universität Erlangen-Nürnberg, Fürther Straße 248, 90429 Nürnberg, Germany.*

E-mail: j.harting@fz-juelich.de; m.sega@fz-juelich.de

Phone: +49 911 32169-102

Abstract

The speculated presence of monomolecular lamellae of antagonistic salts in oil-water mixtures has left several open questions besides their hypothetical existence, including their microscopic structure and stabilization mechanism. Here, we simulate the spontaneous formation of supramolecular aggregates of the antagonistic salt sodium tetraphenylborate (NaBPh₄) in water and 3-methylpyridine (3-MP) at the atomistic level. We show that, indeed, the lamellae are formed by a monomolecular layer of the anion, enveloped by 3-MP and hydrated sodium counterions. To understand which thermodynamic forces drive the aggregation, we compare the full-atomistic model with a simplified one for the salt and show that the strong hydrophobic effect granted by the large excluded volume of the anion, together with electrostatic repulsion, suffice to explain the stability of the monomolecular lamellae.

Introduction

Antagonistic salts are considered a new class of surface-active solutes, with distinct features from the other two known classes, salts and surfactants.¹ Antagonistic salts consist of a relatively large organic ion and a small inorganic

counterion. Unlike typical ionic surfactants, that dissociate into an amphiphilic ion and a small inorganic counterion, the organic ion of an antagonistic salt has a marked preference for organic solvents. In an oil/water mixture, the organic ions are solvated by the oil phase and the inorganic counterions by water, giving rise to the eponymous antagonistic behavior. A typical example of an antagonistic salt and oil mixture is that of NaBPh₄ and 3-MP, as shown in Fig. 1. Thanks to the electrostatic attraction between the organic anion and its counterions, an electric double layer forms at the water/oil interface, providing the surfactant property that manifests itself also by the appearance of typical mesostructures like lamellae.² Oppositely to (homoselective) salts, antagonistic salts also widen the intermiscibility range of their solvent mixtures.^{2,3} Interestingly, theoretical models by Onuki and Kitamura⁴ predicted the appearance of antagonistic salt mesostructures before their experimental observation. Onuki and coworkers' theoretical approach is based on a Ginzburg-Landau mean-field model, which predicts the characteristic wave-like structures as a result of the coupling between solvent and charge concentration.⁴⁻⁶ However, a later analysis showed that the theoretical predictions would fit small-angle neutron scattering (SANS) spectra only using

an unrealistically large Debye length. A better fit to the experimental data could be obtained by using general scattering functions for lamellar structures.⁷

In successive experiments, Sadakane and coworkers studied mixtures of NaBPh₄ in D₂O/3-MP and showed that at salt concentrations larger than 50 mM the two-phase region of D₂O and 3-MP shrinks up to a point where no macroscopic phase separation can be detected at all.⁸ Remarkably, the structures formed by NaBPh₄ reached characteristic lengths close to the wavelength of visible light when the temperature was within a few degrees of the critical point, leading to the observation of mixture coloration that changes sensitively with temperature.⁸ SANS and neutron spin echo measurements confirmed the presence of a disordered phase and, in addition, of an ordered multilamellar vesicle phase at 3-MP volume fractions less than 11%. The thickness of the fluctuating lamellae turned out, surprisingly, to be comparable to the size of the composing BPh₄⁻ anions.⁹ The formation of periodic mesostructures by antagonistic salts has also been confirmed in slightly different solvent mixtures, such as D₂O and dimethylpyridine,¹⁰ and using other salts with similar ionic size asymmetry, such as tetraphenylphosphonium chloride.¹¹

Several mean-field level theoretical and numerical studies have so far delivered some insight into the phase diagram and structure size dependencies of the supramolecular aggregates.¹²⁻¹⁴ In these mean-field studies, the driving force segregating the antagonistic ions into opposite fluid phases is derived from a phenomenological solvation potential varying linearly with the fluid composition. However, little is known so far of the aggregate structure at the molecular scale and about the mechanisms driving mesostructure formation in these mixtures. Motivated by the surprisingly thin, molecular-scale lamellae suggested by the experiments in the ordered phase, which current theoretical models cannot consistently explain, we set out to determine how these lamellar structures form and what stabilizes them by simulating both an atomistic model

of NaBPh₄/3-MP/water ternary mixtures, as well as a mixed atomistic/coarse-grained bead model where each BPh₄⁻ is represented by a single charged interaction point interacting purely repulsively with all others.

Methods

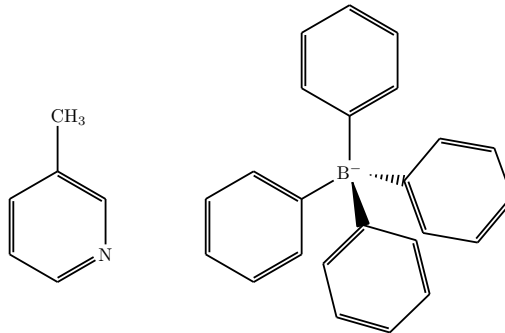


Figure 1: Structure formulae of 3-MP (left) and BPh₄⁻ (right).

Ionic solutions are notoriously difficult to simulate with empirical potentials, where the neglect of charge transfer and electronic polarizability often results in excessive ion pairing and too low solubilities.¹⁵ Charge scaling has proven to be a simple but effective approach to improve the reliability of empirical potentials for ionic systems. Therefore, we modeled sodium ions using the Madrid model, which rescales the charges of anions and cations by a factor of 0.85,¹⁶ in combination with the TIP4P/2005 interaction potential for water,¹⁷ which was used to parametrize the Madrid model. As for the empirical potentials for BPh₄⁻, we started from a template generated by ATB¹⁸ using density functional calculations at the B3LYP/6-31G* level of the theory¹⁹⁻²¹ and the polarizable continuum implicit solvent model.²² Partial charges were assigned using the Merz-Singh-Kollman scheme²³ and scaled by a factor of 0.85 to be consistent with the Madrid model and maintain charge neutrality. We added distance constraints to keep the structure of the molecule rigid, and used the all-atom optimized potential for liquid simulation (OPLS/AA) Lennard-Jones parameters²⁴ as reported in the SI.

As a starting template for 3-MP, we used the topology that Coleman and coworkers used in their benchmark of organic liquid force fields,²⁵ based on OPLS/AA. The thermodynamic properties of the water/3-MP mixture simulated using empirical potentials are known to depend on a delicate balance between the solvation of nitrogen and the dispersion interaction with other 3-MP molecules.²⁶ Experimentally, 3-MP and water mix in every proportion,²⁷ while heavy water and 3-MP produce a closed-loop phase diagram.²⁸ Our preliminary simulations of water/3-MP mixtures using OPLS/AA and TIP4P/2005 revealed an unphysical phase separation at 9% 3-MP volume fraction and all tested temperatures from 250 to 340 K. To improve the quality of the 3-MP model we followed the force field calibration protocol of Salas and coworkers²⁹ by changing the Lennard-Jones parameters and rescaling the original OPLS/AA partial charges of 3-MP atoms until we matched within 7% 3-MP dielectric permittivity,³⁰ density,³¹ and liquid/vapor surface tension³² at 300 K. The new parameterization resulted in a single-phase mixture of water/3-MP in the whole tested range of 3-MP concentrations and temperatures ranging from 10-50 vol% and 275-350 K respectively, as expected for light water. The GROMACS topology files, as well as equilibrated configurations, are available at the central institutional repository for research data of Forschungszentrum Jülich, DOI 10.26165/JUELICH-DATA/OWA443.³³

All our simulations were performed in the isobaric-isothermal ensemble using the Parrinello-Rahman pressure coupling³⁴ and employing the Nosé-Hoover^{35,36} thermostat with relaxation constants of 1.2 and 0.6 ps, respectively. For the fully-atomistic simulations, we took into account the long-range electrostatics and dispersion corrections using the smooth variant of the Particle Mesh Ewald method³⁷ with a grid spacing of 0.12 nm, cubic interpolation scheme, and 10^{-5} and 10^{-4} as relative contribution of the direct part of the electrostatic and Lennard-Jones potential at the cutoff. For the coarse-grained model of BPh_4^- , we computed the Lennard-Jones interaction up to a cutoff distance of $2^{1/6}$ nm.

All simulations were initialized in a cubic simulation cell of either 10 or 24 nm initial side length by randomly placing (taking care of avoiding overlaps) the ions, 3-MP, and eventually water molecules. After an initial energy minimization using the steepest descent algorithm, the systems underwent a preliminary relaxation of 50 ps at a reference pressure of 500 bar to speed up condensation. The systems were further relaxed at a pressure of 1 bar, where the simulation cell edges oscillated around approximately 8 and 20 nm respectively. All simulations were performed using GROMACS 2019³⁸ with an integration step of 2 fs, for a minimum of 50 ns, dumping configurations to disk every 500 ps for subsequent analysis.

Results

Local structure of binary and ternary mixtures

In Fig. 2, we show some snapshots from equilibrated simulations of the ternary solution at different salt concentrations. All snapshots show the full simulation system about 50 ns after initialization from a fully randomly mixed state different for each simulation. The typical structures observed are planar ones in the form of leaflets at low salt concentrations, 2D-spanning membranes at medium salt concentrations, and 3D percolating, bicontinuous structures at high salt content.

Before detailing the composition and structure of these aggregates, it is helpful to understand the role of the different components in the simpler $\text{BPh}_4^-/3\text{-MP}$ and $\text{BPh}_4^-/\text{water}$ binary mixtures.

In $\text{NaBPh}_4/3\text{-MP}$ mixtures the presence of 3-MP is sufficient to fully solvate NaBPh_4 , as a quick look at the boron radial distribution function (RDF) in the top panel of Fig. 3 confirms, although BPh_4^- and Na^+ remain partially associated, with a coordination number of 1.65. 3-MP clearly forms up to two solvation shells around BPh_4^- , as indicated by the dashed curve in the upper panel of Fig. 3.

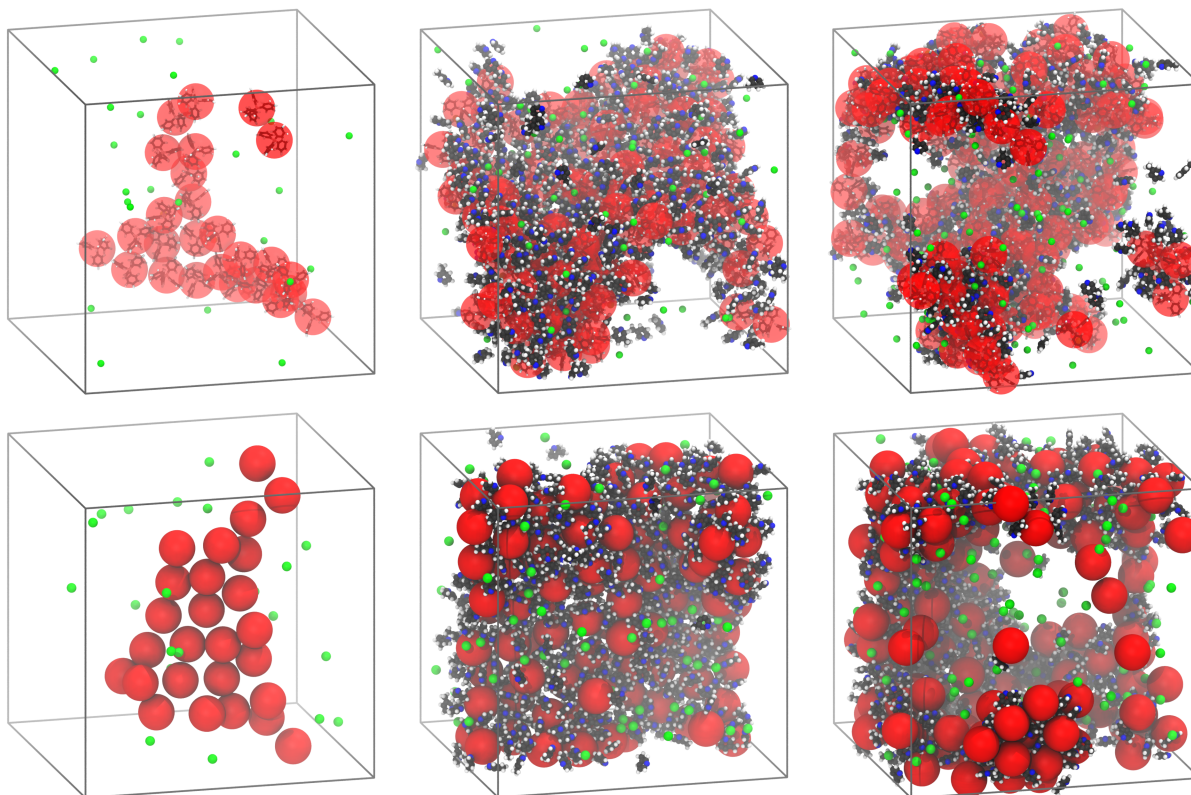


Figure 2: Simulation snapshots of the atomistic (top row) and bead model (bottom row) of NaBPh₄/3-MP/water simulations at $T = 300\text{K}$, 15 vol-% 3-MP and a NaBPh₄ concentration of 80 (left), 300 (center) and 500 mM (right). The snapshots show Na⁺ (green spheres), BPh₄⁻ (sticks representation plus red halo in the atomistic case; red spheres in the bead model case) and 3-MP (balls-and-stick representation). For clarity, water molecules are not shown in any snapshot, and 3-MP is not shown in the 80 mM case.

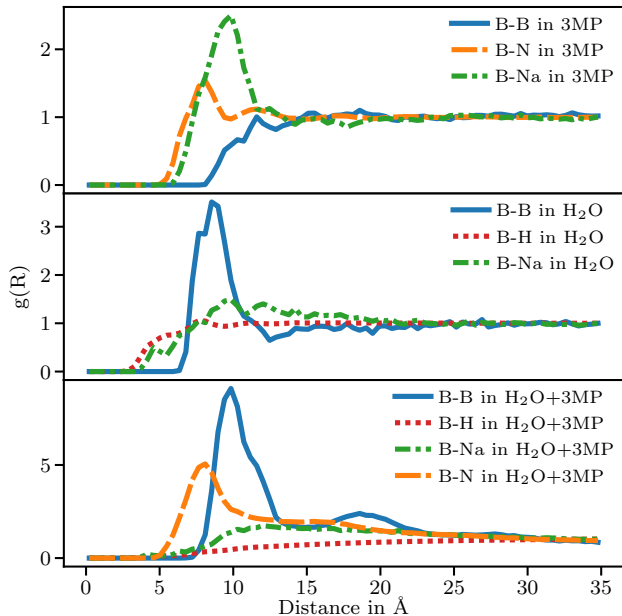


Figure 3: RDFs of 200 mM NaBPh_4 solutions in pure 3-MP (top), pure water (center), and ternary mixture with 15 vol% 3-MP (bottom). N is the nitrogen in 3-MP and H is the hydrogen in water.

On the other hand, NaBPh_4 /water mixtures at low to moderate salt concentrations show the appearance of small, transient structures, mostly pairs or short chains of three BPh_4^- ions. These clusters are responsible for the peak in the boron RDF shown in the central panel of Fig. 3. In this sense, water appears to be a worse solvent for NaBPh_4 than 3-MP. This is somewhat surprising because 3-MP has a noticeably weaker dipole moment than water. However, one needs to consider the fact that water can fully dissociate the NaBPh_4 into solvated ion pairs. In contrast, a significant number of ion pairs persist in 3-MP, as shown by the coordination number. The formation of transient pairs and short chains of BPh_4^- can be attributed to the hydrophobic character of the large BPh_4^- ion, where the charge of boron is buried behind the four phenyl rings.

When the ternary mixture is considered, the boron RDF changes dramatically, showing a much more prominent primary peak and a sizeable secondary peak. Together with the slow decay of all correlation functions, these two peaks suggest the presence of extended clus-

ters with a dimensionality lower than 3. From the detail of the cross-sectional structure shown in Fig. 4 as well as from the boron-nitrogen RDF in the bottom panel of Fig. 3, it is clear that 3-MP envelops the BPh_4^- aggregates with one molecular layer. Here BPh_4^- displays hydrotropic behavior, since it aggregates much more than in either pure water or pure 3-MP.

The primary peak of the boron RDF shifts by 0.1 nm to larger distances as compared to the case of water only. One could argue that due to the presence of surrounding 3-MP, the charges of BPh_4^- interact effectively through a medium with lower dielectric permittivity than water, therefore repelling each other more intensely. However, neither water nor 3-MP is found between neighboring BPh_4^- ions. Therefore, the dielectric mismatch of the microphases may be an incomplete explanation of the larger ion separation.

In the ternary solution the distribution of 3-MP is peaked more closely to BPh_4^- than that of Na^+ counterions, similarly to the NaBPh_4 /3-MP case. In the ternary solution, however, NaBPh_4 pairs are almost always dissociated because of the strong preference of Na^+ for the aqueous environment.

Clearly the combination of both solvents, water and 3-MP, is needed for NaBPh_4 to form supramolecular structures, with the crucial steps being (1) the separation of Na^+ from its counterion due to solvation by water, and (2) the hydrotropic action of 3-MP enabling the formation of a combined hydrophobic aggregate with BPh_4^- , whose shape is modulated by both the salt concentration and the 3-MP volume fraction.

Morphology of NaBPh_4 /3-MP aggregates

Across a broad range of salt and 3-MP concentrations, we found that mesostructures in ternary mixtures consist of the same building block exemplified in Fig. 4, namely BPh_4^- leaflets enveloped in one layer of 3-MP. The leaflets deform strongly under thermal fluctuations and sometimes form transient vesicles when these fluctuations bring opposing ends of

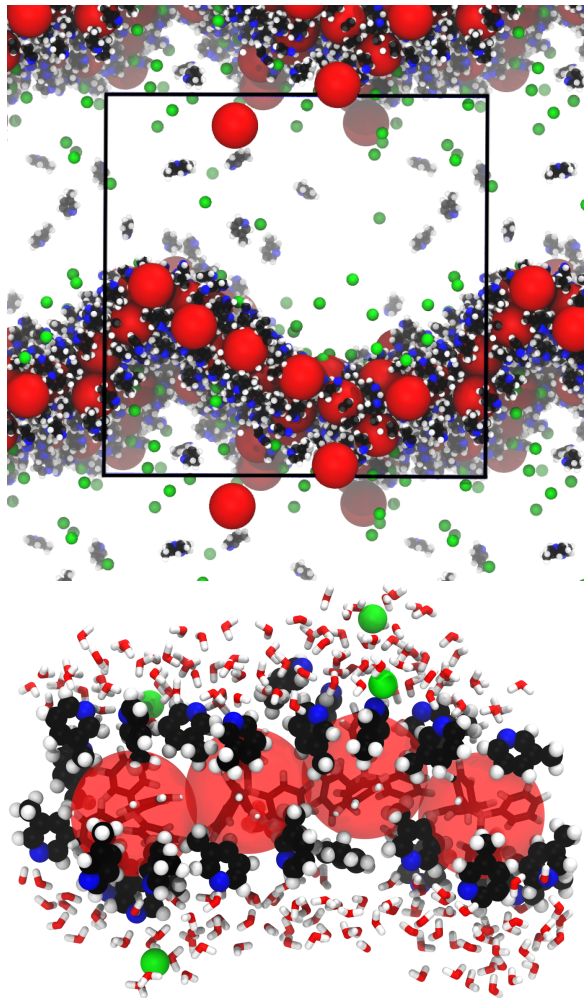


Figure 4: Leaflet cross section at 15 vol% 3-MP and 300 mM salt (top: bead model, bottom: atomistic model, detail) showing BPh_4^- (red spheres, sticks plus red halo), Na^+ (green spheres), 3-MP (ball-and-stick representation), and water (sticks). Water molecules in the top panel have been removed for clarity. The black lines mark the simulation box.

a leaflet into contact, occasionally enveloping one or more Na^+ ions, which could reduce the electrostatic self-repulsion of the BPh_4^- anions. An example of such a vesicle is shown in Fig. S1 in the SI. The structures observed in the 8 nm edge length systems were also present in larger simulations (edge length 20 nm) that we performed on the JUWELS supercomputing cluster³⁹ and used to test for finite-size effects. Results from these larger simulations are likewise shown in the SI in Fig. S2.

As a general rule, smaller concentrations lead to the formation of smaller leaflets. Already at salt concentrations of 210 mM, leaflets span the entire simulation box even in the 20 nm systems.

We occasionally observed stable holes, about 5 BPh_4^- in size, in some of the lamellar structures both in the small and in the large simulation box. This suggests that the observed holes are not an artifact of the periodic boundaries, but a genuine feature. Tasio and coworkers observed similar structures in their lattice-based coarse-grained Monte Carlo simulations of antagonistic salt mixtures.¹³ The authors found the structure factor of these perforated leaflets to be practically indistinguishable from that of unperforated leaflets, rendering both types of structures plausible explanations of the experimentally observed ordered lamellar structures.⁹

The leaflet structure becomes less discernible at high salt concentrations, as the BPh_4^- anions form complicated three-dimensionally branched structures reminiscent of a sponge phase. Still, the aggregates can be described as strongly curved interconnected leaflets or chains with thicknesses not exceeding one or two BPh_4^- anions.

These structures would explain the experimental observations made by Sadakane and coworkers at salt concentrations larger than 300 mM, where the authors found a single peak in the SANS structure factor suggesting a sponge phase with a lamellar width of about 1.6 nm, that is, about one and a half times the diameter of BPh_4^- . Unlike in the patterns measured at lower concentrations, no secondary Bragg peaks were detected at concentrations larger than 300 mM, indicating the disappear-

ance of periodic lamellar arrangements.⁹

As already mentioned, lamellae at all concentrations consist of a leaflet of BPh_4^- anions enveloped by a thin layer of 3-MP, with the overwhelming majority of Na^+ cations solvated in the water phase. As a result, the lamellae are negatively charged with a surface charge density that can be estimated from the local arrangement of BPh_4^- ions to be about $1.0 e/\text{nm}^2$, with e the electron charge.

It is worth noting that one key ingredient in the leaflet formation is the size of the Na^+ counterions. If one uses Na^+ counterions with a Lennard-Jones energy parameter 20 times smaller than the correct one, the counterions' reduced effective size allows them to fit, together with their first water hydration shell, between the phenyl rings of BPh_4^- ion pairs. As soon as Na^+ ions infiltrate the BPh_4^- leaflets, the electrostatic self-repulsion no longer limits the growth of the BPh_4^- clusters in volume, and spherical aggregates are formed in place of leaflets. An example of such a spherical aggregate is shown in Fig. S3. When, on the other hand, there is no room in the hydrophobic $\text{BPh}_4^-/3\text{-MP}$ clusters for Na^+ ions and their solvation shells, Na^+ counterions remain in the aqueous phase. The aggregates try to maximize their interfacial surface area to minimize the electrostatic energy cost associated with a spatial separation of the ionic charges, eventually leading to the formation of leaflets.

From these results, one can appreciate the complex and delicate interplay between the various species' solvation forces, inducing aggregation of the otherwise mixing 3-MP in water as soon as it is combined with NaBPh_4 . In turn, NaBPh_4 in pure 3-MP does not aggregate because 3-MP is not polar enough to trigger the hydrophobic effect. In pure water, NaBPh_4 would be close to the size limit of forming hydrophobic aggregates if it were neutral, even in the absence of dispersion forces.⁴⁰ However, in this case, the electrostatic interaction provides sufficient repulsion to prevent aggregation beyond the formation of pairs or triplets at all but the highest salt concentrations.

Bead model of BPh_4^-

To investigate the role of the hydrophobic effect in driving the aggregation, we repeated our simulations using a simplified bead model of NaBPh_4 . In this model, we represent the complex BPh_4^- ion with a charged, pointlike particle, interacting with other BPh_4^- ions via Coulomb and purely repulsive Lennard-Jones potentials only. In this way, we aim to exclude the contribution from attractive dispersion forces between BPh_4^- ions and any influence from their molecular structure.

In this sort of partial coarse-graining approach, each BPh_4^- bead is assigned a charge of $0.85 e$, a Lennard-Jones potential with energy parameter $\epsilon=1.47 \text{ kJ/mol}$ (the same value from the Madrid model we used in the atomistic model for Na^+), and a Lennard-Jones diameter $\sigma=1 \text{ nm}$. The other ions and molecules were modeled in the same way as in the previous simulations. In the case of this bead model, however, we truncated the Lennard-Jones interaction at the minimum of the potential (at a distance of $2^{1/6} \simeq 1.122 \text{ nm}$), thus implementing the purely repulsive Weeks-Chandler-Andersen potential⁴¹ for the coarse-grained BPh_4^- ions. Since the Lennard-Jones diameters of all other atoms are much smaller than 1 nm, all other interactions can be considered by all practical means the same as in the fully atomistic model.

As we demonstrate for three concentrations in Fig. 2, the structures we obtain with this simple bead model are almost identical to those obtained with the fully atomistic NaBPh_4 one. This shows that neither specific BPh_4^- - BPh_4^- attractive interaction, nor some kind of interlocking of the phenyl rings is needed to obtain the monomolecular BPh_4^- layers. It is noteworthy that the size of the BPh_4^- anions (1 nm) lies exactly at the crossover between entropy- and enthalpy-dominated regimes of the solvation free energy.⁴⁰ Stable or metastable aggregates can form spontaneously (in water) only when a cluster exceeds the size threshold of 1 nm. Therefore, BPh_4^- ions can directly act as hydrophobic building blocks for the monomolecular lamellae and do not first need to form primary aggregates that would in turn assem-

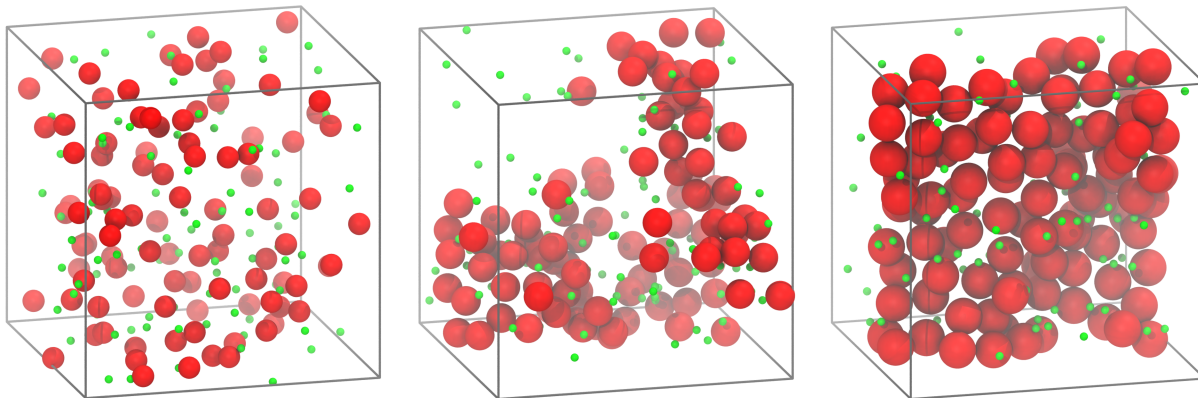


Figure 5: Snapshots from bead model simulations at 15% 3-MP and 300 mM salt with large bead diameter $\sigma = 0.6$ nm (left) and $\sigma = 0.8$ nm (center), and $\sigma = 1$ nm (right). Anions (red) and cations (green) both shown to scale.

ble into a thicker aggregate. This view is confirmed, as we show in Fig. 5, by the fact that even a slight decrease of the BPh_4^- bead size to $\sigma=0.8$ nm strongly disrupts the leaflet shape. Upon a further decrease to $\sigma=0.6$ nm, BPh_4^- aggregation practically ceases completely.

This strong dependence of structure formation on the size of the larger ion is consistent with experimental results from small-angle X-ray scattering by Witala and coworkers using mixtures of water, dimethylpyridine and 10 mM of tetra-*n*-alkylammonium bromide salt, whose cation was varied in size via the length of hydrocarbon chains attached to it. By fitting a structure factor based on theory results from Onuki and Kitamura⁴ to their scattering spectra, they observed that the coupling of the ions to opposite solvent phases becomes sufficiently strong to enable the formation of periodic structures around a size contrast slightly smaller than that between sodium and tetraphenylborate.⁴²

Accessible surface area

To quantify how well the structures conform to a leaflet shape and how accurately the atomistic and bead model results coincide, we performed measurements of the accessible molecular surface area (ASA)⁴³ as implemented in the freely available `pytim` analysis package.⁴⁴ By comparing the measured ASA values with those calculated from two simple models (planar leaflets and spherical micelles), we obtain

a useful gauge to quantify whether our simplified picture of the molecular arrangement can or cannot be considered a fitting description. In these models we assume the BPh_4^- anions to be beads with a radius $R = 0.5$ nm arranged in hexagonal close packing on a plane or in a sphere.

In a first step we numerically calculated the average ASA per particle as a function of the number N of aggregated particles in either planar or spherical close packing. For this purpose we placed particles in either a 2D or 3D hexagonal lattice and then selected the closest N particles around some arbitrary point in the lattice. The obtained ASA as a function of N is described well by simple power law fits, as shown in Fig. S4.

Fig. 6 reports a comparison of the measured ASA for both the bead model and the atomistic simulations with the idealized models of planar leaflets and spherical micelles with the same cluster size distribution as in the simulations. To make the measured ASA of the bead and fully atomistic models comparable, we measured in the atomistic simulations the ASA of spheres of 0.5 nm radius centered on each BPh_4^- anion.

The bead and fully atomistic models yield very similar ASA values for all concentrations.

In the central panels of Fig. 2 we can see that the lamella obtained in the bead model connects with itself completely through the periodic boundaries, leading to the absence of bor-

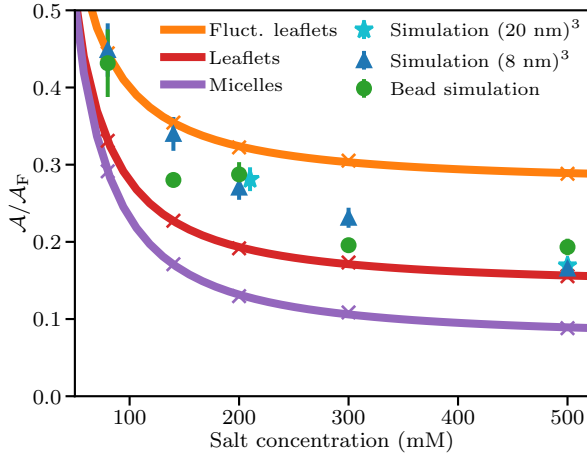


Figure 6: ASA \mathcal{A} per BPh_4^- accessible to a test sphere of 0.5 nm radius, as a function of NaBPh_4 concentration. Normalized by full surface \mathcal{A}_F of a 0.5 nm BPh_4^- bead. All simulation results from trajectories at 15 vol% of 3-MP. Error bars show standard deviation over 25 ns.

der particles and hence a smaller ASA, whereas the atomistic model lamella does not contain enough material to fill the larger diagonal cross-section of the simulation box. While the size and shape of the simulation box can clearly lead to some degree of variation in the measured ASA, the good agreement between simulations in 8 nm systems and those in 20 nm systems suggests that larger system sizes do not systematically change the obtained results.

The theoretical values in the leaflet and spherical cluster models decrease with concentration because of the increasing size of the clusters and a corresponding decrease in the ratio of border/inner molecules. The simple leaflet model predicts ASA values that lie below those obtained in simulation for all concentrations. This deviation can be qualitatively explained by the presence of thermal fluctuations displacing individual BPh_4^- beads perpendicular to the local leaflet plane and thus coarsening the leaflet surface. The fluctuating leaflet model in Fig. 6 shows the substantial increase in ASA induced by adding a normally distributed displacement perpendicular to the plane with a standard deviation equal to one particle radius to each particle in the leaflet model. While the amplitude of this displacement is chosen somewhat arbi-

trarily, the resulting model leaflet shapes look quite similar to the fluctuating leaflets obtained in simulations, as shown in Fig. S4. Besides the influence of thermal fluctuations, the ASA is also increased at small salt concentration due to a non-circular, frayed shape of the leaflets (compare Fig. 2).

The good agreement between the leaflet model and the measured ASA at high salt concentration in Fig. 6 does not mean that the leaflets here are unperturbed by fluctuations. Beyond about 200 mM of NaBPh_4 , the leaflets in both the 8 nm and 20 nm systems start connecting with their periodic images, becoming effectively infinite objects with no exposed boundary particles and, therefore, a lower ASA. This decrease in the number of border particles is not reproduced in the leaflet model, which does not take periodic boundary conditions into account. Furthermore, large salt concentrations lead to an increased frequency of local imperfections in coplanar particle arrangement due to crowding.

The average number of neighboring BPh_4^- anions surrounding each BPh_4^- within a 1.25 nm cutoff is 4.0 ± 1.4 , 4.8 ± 1.3 , 5.4 ± 1.2 , 5.7 ± 1.4 , and 6.3 ± 1.7 at 80, 140, 200, 300, and 500 mM BPh_4^- , respectively. One has to consider that the fraction of BPh_4^- at the border of the aggregates (thus with fewer neighbors than 6) is higher at lower concentrations, thus decreasing the average number of neighbors. The fraction of BPh_4^- in the system with a number of neighbors between 3 and 6, which can be considered consistent with a planar hexagonal arrangement taking into account border particles, is 79% (80 mM), 89% (140 mM), 80% (200 mM), 70% (300 mM), and 56% (500 mM). At high salt concentrations, a growing fraction of particles has 7 or 8 neighbors due to surface-adsorbed additional BPh_4^- particles or intersections between distinct leaflets in the sponge phase.

In summary, the measured ASA values and cluster statistics confirm the picture suggested by visual inspection, of a locally planar particle arrangement perturbed by thermal fluctuations and crowding defects in a relatively broad range of concentrations.

To interpret the ASA results further, we

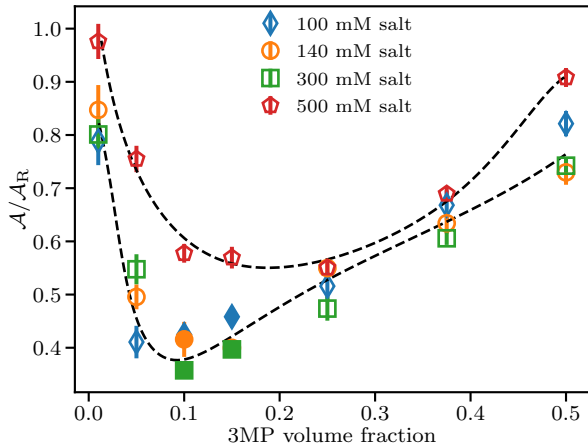


Figure 7: ASA \mathcal{A} per BPh_4^- accessible to a test sphere of 0.5 nm radius, as a function of 3-MP volume fraction. Results normalized by expected ASA \mathcal{A}_R under random particle distribution. The dashed lines are spline fits and serve only as guides to the eye. Filled symbols mark lamellar phase structures. Error bars show standard deviation over 25 ns.

found it helpful to introduce the concept of the ASA \mathcal{A}_R of a random distribution of BPh_4^- beads. In practice, we determined the function \mathcal{A}_R as the best fit of a power law (similarly to the case of the leaflet and micelle models) to the ASA values of randomly placed non-overlapping spheres in 3D.

The ASA at salt concentrations up to 300 mM seems to decrease following about the same functional form as \mathcal{A}_R . In fact, in Fig. 7, $\mathcal{A}/\mathcal{A}_R$ is only weakly dependent on the salt concentration, except for the 500 mM case. Even though \mathcal{A} is smaller at 500 mM than at lower salt concentrations, it is comparatively closer to the ASA \mathcal{A}_R of a random distribution. Correspondingly, $\mathcal{A}/\mathcal{A}_R$ is the largest at 500 mM. Dense clustering of BPh_4^- eventually becomes unavoidable for purely entropic reasons as the salt volume fraction increases, and $\mathcal{A}/\mathcal{A}_R \approx 1$ is to be expected regardless of interparticle interactions when BPh_4^- concentrations approach close packing. At 500 mM, the volume fraction of BPh_4^- , represented by 0.5 nm beads, reaches about 16%. Crowding at high salt concentrations apparently induces a particle arrangement slightly more similar to random placement in-

stead of the entropically costly generation of separate lamellae.

Small values of $\mathcal{A}/\mathcal{A}_R \ll 1$ indicate that aggregation is enhanced by effective interparticle interactions rather than occurring merely due to volume constraints. With this interpretation in mind, Fig. 7 suggests that 3-MP concentrations in the range of 10-15 vol-%, where the lamellar phase is observed, yield ideal conditions for the hydrophobic aggregation of BPh_4^- . Both at larger and smaller 3-MP volume fractions BPh_4^- tends to cluster less densely, leaving a larger ASA.

Phase diagram

Fig. 8 presents a phase diagram that summarizes our findings. As indicated in Fig. 7, both small and large 3-MP concentrations are detrimental to the aggregation of BPh_4^- , so that only disordered arrangements of dissolved BPh_4^- anions are observed at both extremes of 3-MP concentration. Approaching the limit of NaBPh_4 solvation in pure water, BPh_4^- forms only small, transient clusters because the electrostatic self-repulsion of BPh_4^- impedes the growth of large hydrophobic aggregates without the assistance of the moderately hydrophobic 3-MP. When there is a surplus of 3-MP in the system, on the other hand, the lack of water makes the formation of hydrophobic BPh_4^- clusters unnecessary. BPh_4^- can loosely dissolve in 3-MP-rich microphases without discernible ordering, avoiding the entropic and electrostatic energy costs associated with a compact arrangement of BPh_4^- anions.

In Fig. 8, we label any structure as belonging to the sponge phase that connects to itself through periodic boundaries in all three dimensions and consists of intersecting leaflets and/or chains with a thickness not regularly exceeding one BPh_4^- . The sponge phase consistently exhibits a monomolecular leaflet microstructure at higher 3-MP concentrations, as in the example shown in Fig. 8. Note that any seemingly isolated BPh_4^- particles in the example shown in Fig. 8 form part of a leaflet structure when the periodic boundaries are taken into account.

Just like the lamellar phase, the chain phase

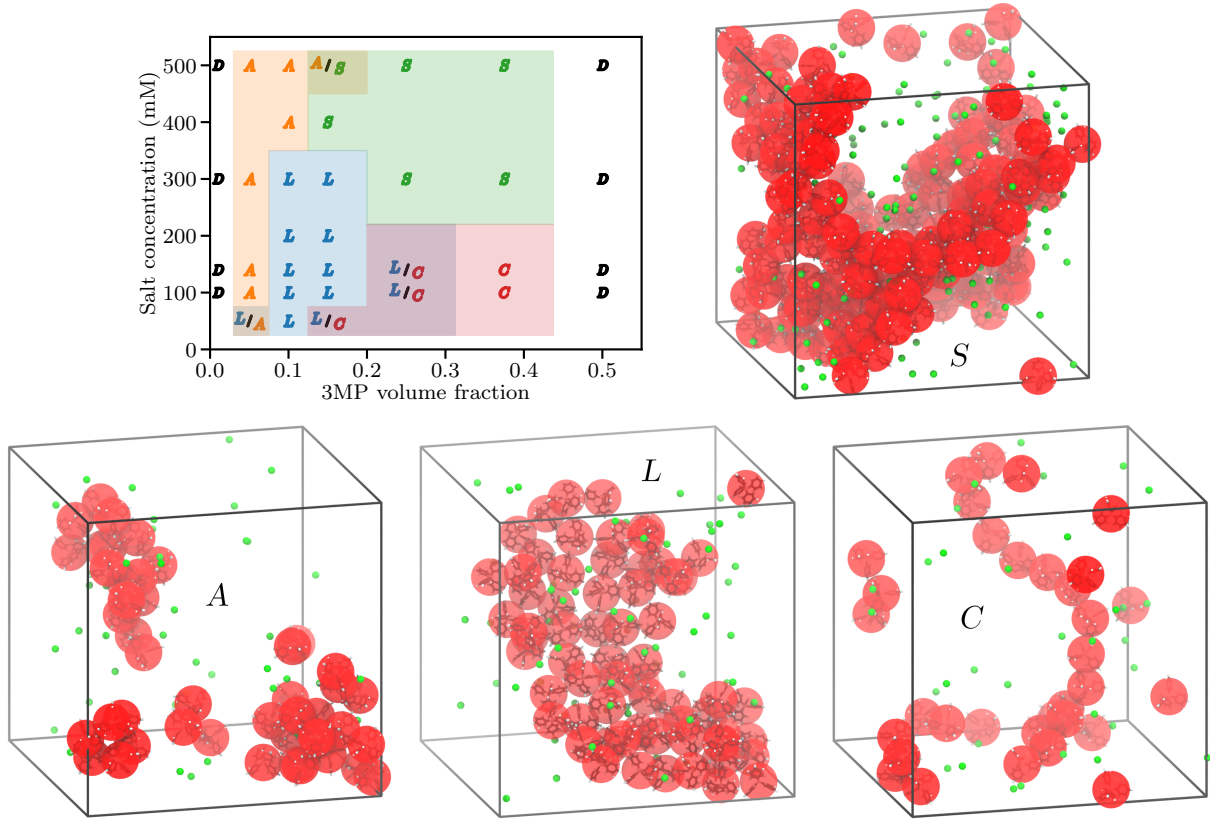


Figure 8: Phase diagram of NaBPh₄/3-MP/water mixture interpreted from atomistic 8 nm simulations. *D* stands for disordered arrangements, where BPh₄⁻ is mostly randomly distributed, *S* stands for the sponge phase (see upper right pane for 25% 3-MP and 500 mM salt), consisting of 3D interconnected leaflets and chains, *C* stands for chains (see lower right pane for 37.5% 3-MP and 100 mM salt), *L* stands for the lamellar phase, i.e. planar leaflets (see lower center pane for 10% 3-MP and 200 mM salt), and *A* stands for amorphous aggregates (see lower left pane for 5% 3-MP and 140 mM salt).

that occurs at large 3-MP but small salt concentrations turns into the sponge phase at higher salt concentrations. Compared to the lamellar phase, the chain phase turns into the sponge phase at slightly lower salt concentrations. This can be understood as a consequence of the decreased pressure for the BPh_4^- aggregates to limit their surface area in order to avoid the water phase when there is little water in the system.

To the best of our knowledge the chain phase has not been yet identified in experiments. The majority of experimental studies on NaBPh_4 mesophases so far have focused on the 3-MP concentration range in which the lamellar phase is observable, due to its characteristic Bragg peaks visible in SANS scattering. Sadakane et al. performed some SANS measurements in a parameter range corresponding to the appearance of chain structures in our simulations, but, unfortunately, they could not extract any details about the microstructure of the observed phases apart from a characteristic periodicity of about 6 to 10 nm,⁸ leaving the question of the existence of this phase open.

The lamellar phase has been discussed in detail in the previous sections. Fig. 8 shows an additional example of a lamella exhibiting a large degree of bending due to thermal fluctuations. At different stages of the simulation this bending almost caused the lamella to wrap around and form a spherical, vesicle-like shape comparable to Fig. S1. A few deviations from a perfectly monomolecular leaflet are visible near the bottom of the illustration, where individual BPh_4^- particles have aggregated on top of the lamella.

The phase of amorphous aggregates is characterized by structures without a particular geometry, with a thickness often exceeding one BPh_4^- . When 3-MP is scarce in the system, the formation of hydrophobic clusters with BPh_4^- can still be observed, but 3-MP is not sufficiently available to envelop a planar BPh_4^- leaflet, forcing the BPh_4^- aggregates to form thicker aggregates despite their electrostatic repulsion.

The transition regions between the phases are occasionally ambiguous. Simulations contain-

ing either several aggregates pertaining to different phases or single aggregates deforming in time to resemble either one phase or the other were labeled as pertaining to both phases. At salt concentrations below about 100 mM the average size of clusters decreases, making it progressively more difficult to distinguish the different phases.

Conclusions

We showed that monomolecular leaflets of BPh_4^- appear in ternary NaBPh_4 /3-MP/water mixtures, forming lamellae stabilized by a substantial surface charge when the salt concentration is up to 300 mM and the 3-MP concentration is about 10-15 vol%. The leaflets consist of one layer of BPh_4^- ions enveloped by one molecular layer of 3-MP on either side and a cloud of Na^+ counterions solvated by water.

The leaflet thickness, including both BPh_4^- and 3-MP, can be estimated from the boron-nitrogen radial distribution functions to be approximately 1.6 nm. These observations agree with the presence of lamellae with a thickness of about 1.5 ± 0.5 nm at similar salt and 3-MP concentrations suggested by SANS data.⁹ Our simulations suggest that lamellae form if enough 3-MP is available to envelop the BPh_4^- leaflets, but not as much as to provide a large surplus of 3-MP in the surrounding solvent, as this would encourage BPh_4^- to form aggregates with a larger surface to volume ratio, such as chains of individual BPh_4^- . Also, the BPh_4^- concentration should be large enough to allow for the aggregation of enough BPh_4^- to form a large leaflet, but not as much to reach the sponge phase.

We have also shown that practically identical structures can be obtained by replacing the fully atomistic model of BPh_4^- ions with a simpler model of charged, repulsive spheres. The leaflet formation and stabilization can be explained simply by considering the ionic charge and the hydrophobic effect, without the need for attractive dispersion forces between the BPh_4^- ions.

In this sense, we expect that mixtures with

similar properties could be realized by employing as three main ingredients (1) a salt with large size difference between anion and cation, with one of the two larger than the 1 nm critical threshold for hydrophobic aggregation (2) a moderately polar co-solvent exhibiting hydrotropic features and (3) a polar solvent like water.

Supporting information

Includes additional figures depicting larger simulations and structural details, as well as links to our simulation data and topologies used.

Acknowledgments

The authors gratefully acknowledge the Gauss Centre for Supercomputing e.V. (www.gauss-centre.eu) for funding this project by providing computing time on the GCS Supercomputer JUWELS at Jülich Supercomputing Centre (JSC).

References

- (1) Michler, D.; Shahidzadeh, N.; Westbrook, M.; van Roij, R.; Bonn, D. Are Antagonistic Salts Surfactants? *Langmuir* **2015**, *31*, 906–911.
- (2) Sadakane, K.; Seto, H.; Nagao, M. Long-Range Periodic Structure Induced by Coupling of the Solvation Effect and Concentration Fluctuation in Water and 3-Methylpyridine With Salts. *Chem. Phys. Lett.* **2006**, *426*, 61–65.
- (3) Glende, G.; de Wijn, A. S.; Pousaneh, F. The Vanishing Water/Oil Interface in the Presence of Antagonistic Salt. *J. Chem. Phys.* **2020**, *152*, 124707.
- (4) Onuki, A.; Kitamura, H. Solvation Effects in Near-Critical Binary Mixtures. *J. Chem. Phys.* **2004**, *121*, 3143–3151.
- (5) Onuki, A.; Okamoto, R.; Araki, T. Phase Transitions in Soft Matter Induced by Selective Solvation. *B. Chem. Soc. Jpn.* **2011**, *84*, 569–587.
- (6) Onuki, A.; Yabunaka, S.; Araki, T.; Okamoto, R. Structure Formation Due to Antagonistic Salts. *Curr. Op. Coll. Inter. Sci.* **2016**, *22*, 59–64.
- (7) Sadakane, K.; Seto, H.; Endo, H.; Kojima, M. Mesoscopic Structure in Near-Critical Mixtures of D2O and 3-Methylpyridine With Salts. *J. Appl. Crystallogr.* **2007**, *40*, 527–531.
- (8) Sadakane, K.; Seto, H.; Endo, H.; Shibayama, M. A Periodic Structure in a Mixture of D2O/3-Methylpyridine/NaBPh4 Induced by Solvation Effect. *J. Phys. Soc. Jpn.* **2007**, *76*, 113602.
- (9) Sadakane, K.; Nagao, M.; Endo, H.; Seto, H. Membrane Formation by Preferential Solvation of Ions in Mixture of Water, 3-Methylpyridine, and Sodium Tetrphenylborate. *J. Chem. Phys.* **2013**, *139*, 234905.
- (10) Sadakane, K.; Endo, H.; Nishida, K.; Seto, H. Lamellar/Disorder Phase Transition in a Mixture of Water/2,6-Dimethylpyridine/Antagonistic Salt. *J. Solution Chem.* **2014**, *43*, 1722–1731.
- (11) Sadakane, K.; Horikawa, Y.; Nagao, M.; Seto, H. The Effect of Tetraphenylphosphonium Chloride on Phase Behavior and Nanoscale Structures in a Mixture of D2O and 3-Methylpyridine. *Chem. Lett.* **2012**, *41*, 1075–1077.
- (12) Araki, T.; Onuki, A. Dynamics of Binary Mixtures With Ions: Dynamic Structure Factor and Mesophase Formation. *J. Phys. Cond. Matt.* **2009**, *21*, 424116.
- (13) Tasios, N.; Samin, S.; van Roij, R.; Dijkstra, M. Microphase Separation in Oil-Water Mixtures Containing Hydrophilic and Hydrophobic Ions. *Phys. Rev. Lett.* **2017**, *119*, 218001.

- (14) Jung, D.; Rivas, N.; Harting, J. How Antagonistic Salts Cause Nematic Ordering and Behave Like Diblock Copolymers. *J. Chem. Phys.* **2019**, *150*, 064912.
- (15) Smith, W. R.; Nezbeda, I.; Kolafa, J.; Moučka, F. Recent Progress in the Molecular Simulation of Thermodynamic Properties of Aqueous Electrolyte Solutions. *Fluid Phase Equilib.* **2018**, *466*, 19–30.
- (16) Benavides, A. L.; Portillo, M. A.; Chamorro, V. C.; Espinosa, J. R.; Abascal, J. L. F.; Vega, C. A Potential Model for Sodium Chloride Solutions Based on the TIP4P/2005 Water Model. *J. Chem. Phys.* **2017**, *147*, 104501.
- (17) Abascal, J. L. F.; Vega, C. A General Purpose Model for the Condensed Phases of Water: TIP4P/2005. *J. Chem. Phys.* **2005**, *123*, 234505.
- (18) Malde, A. K.; Zuo, L.; Breeze, M.; Stroet, M.; Poger, D.; Nair, P. C.; Oostenbrink, C.; Mark, A. E. An Automated Force Field Topology Builder (ATB) and Repository: Version 1.0. *J. Chem. Theory Comput.* **2011**, *7*, 4026–4037.
- (19) Becke, A. D. Density-Functional Thermochemistry. III. The Role of Exact Exchange. *J. Chem. Phys.* **1993**, *98*, 5648–5652.
- (20) Lee, C.; Yang, W.; Parr, R. G. Development of the Colle-Salvetti Correlation-Energy Formula Into a Functional of the Electron Density. *Phys. Rev. B* **1988**, *37*, 785.
- (21) Perdew, J. P.; Wang, Y. Accurate and Simple Analytic Representation of the Electron-Gas Correlation Energy. *Phys. Rev. B* **1992**, *45*, 13244.
- (22) Miertuš, S.; Scrocco, E.; Tomasi, J. Electrostatic Interaction of a Solute with a Continuum. A Direct Utilization of Ab Initio Molecular Potentials for the Prediction of Solvent Effects. *Chem. Phys.* **1981**, *55*, 117–129.
- (23) Singh, U. C.; Kollman, P. A. An Approach to Computing Electrostatic Charges for Molecules. *J. Comp. Chem.* **1984**, *5*, 129–145.
- (24) Jorgensen, W. L.; Tirado-Rives, J. Potential Energy Functions for Atomic-Level Simulations of Water and Organic and Biomolecular Systems. *Proc. Natl. Acad. Sci. USA* **2005**, *102*, 6665–6670.
- (25) Caleman, C.; van Maaren, P. J.; Hong, M.; Hub, J. S.; Costa, L. T.; van der Spoel, D. Force Field Benchmark of Organic Liquids: Density, Enthalpy of Vaporization, Heat Capacities, Surface Tension, Isothermal Compressibility, Volumetric Expansion Coefficient, and Dielectric Constant. *J. Chem. Theory Comput.* **2012**, *8*, 61–74.
- (26) Almásy, L.; Bánki, P.; Bellissent-Funel, M.; Bokor, M.; Cser, L.; Jancsó, G.; Tompa, K.; Zanotti, J. QENS and NMR Studies of 3-Picoline–Water Solutions. *Appl. Phys. A* **2002**, *74*, 516–518.
- (27) Andon, R. J. L.; Cox, J. D. Phase Relationships in the Pyridine Series. Part I. The Miscibility of Some Pyridine Homologues with Water. *J. Chem. Soc.* **1952**, 4601–4606.
- (28) Cox, J. D. Phase Relationships in the Pyridine Series. Part II. The Miscibility of Some Pyridine Homologues with Deuterium Oxide. *J. Chem. Soc.* **1952**, 4606–4608.
- (29) Salas, F. J.; Méndez-Maldonado, G. A.; Núñez-Rojas, E.; Aguilar-Pineda, G. E.; Domínguez, H.; Alejandre, J. Systematic Procedure To Parametrize Force Fields for Molecular Fluids. *J. Chem. Theory Comput.* **2015**, *11*, 683–693.
- (30) Madelung, O., Ed. *Static Dielectric Constants of Pure Liquids and Binary Liquid Mixtures*; Supplement to Landolt-Börnstein - Group IV Physical Chemistry; Springer-Verlag: Berlin/Heidelberg, 1991.

- (31) Haynes, W. M.; Lide, D. R.; Bruno, T. J. *CRC Handbook of Chemistry and Physics*, 97th ed.; CRC Press: London/New York, 2016.
- (32) Wohlfarth, C. In *Surface Tension of Pure Liquids and Binary Liquid Mixtures: Supplement to Volume IV/24*; Lechner, M. D., Ed.; Physical Chemistry; Springer-Verlag: Berlin/Heidelberg, 2016.
- (33) Jung, D.; Harting, J.; Sega, M. Monolayer Structure of Supramolecular Antagonistic Salt Aggregates - Topologies and Configurations. 2021; <https://doi.org/10.26165/JUELICH-DATA/OWA443>.
- (34) Parrinello, M.; Rahman, A. Polymorphic Transitions in Single Crystals: A New Molecular Dynamics Method. *J. Appl. Phys.* **1981**, *52*, 7182–7190.
- (35) Nosé, S. A Molecular Dynamics Method for Simulations in the Canonical Ensemble. *Mol. Phys.* **1984**, *52*, 255–268.
- (36) Hoover, W. G. Canonical Dynamics: Equilibrium Phase-Space Distributions. *Phys. Rev. A* **1985**, *31*, 1695–1697.
- (37) Essmann, U.; Perera, L.; Berkowitz, M. L.; Darden, T.; Lee, H.; Pedersen, L. G. A Smooth Particle Mesh Ewald Method. *J. Chem. Phys.* **1995**, *103*, 8577–8593.
- (38) Abraham, M. J.; Murtola, T.; Schulz, R.; Páll, S.; Smith, J. C.; Hess, B.; Lindahl, E. GROMACS: High Performance Molecular Simulations Through Multi-Level Parallelism from Laptops to Supercomputers. *SoftwareX* **2015**, *1-2*, 19–25.
- (39) Jülich Supercomputing Centre, JUWELS: Modular Tier-0/1 Supercomputer at the Jülich Supercomputing Centre. *Journal of large-scale research facilities* **2019**, *5*.
- (40) Chandler, D. Interfaces and the Driving Force of Hydrophobic Assembly. *Nature* **2005**, *437*, 640–647.
- (41) Weeks, J. D.; Chandler, D.; Andersen, H. C. Role of Repulsive Forces in Determining the Equilibrium Structure of Simple Liquids. *J. Chem. Phys.* **1971**, *54*, 5237–5247.
- (42) Witala, M.; Lages, S.; Nygård, K. Mesoscale Ordering in Binary Aqueous Solvents Induced by Ion Size Asymmetry. **2016**, *12*, 4778–4782.
- (43) Lee, B.; Richards, F. M. The Interpretation of Protein Structures: Estimation of Static Accessibility. *J. Mol. Biol.* **1971**, *55*, 379–400.
- (44) Sega, M.; Hantal, G.; Fábíán, B.; Jedlovský, P. Pytim: A Python Package for the Interfacial Analysis of Molecular Simulations. *J. Comput. Chem.* **2018**, *39*, 2118–2125.

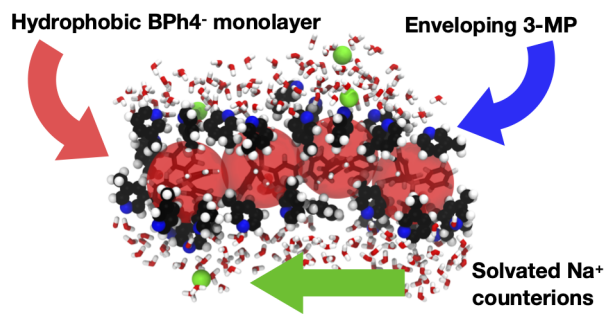


Figure 9: For Table of Contents Only